Deep tissue two-photon microscopy

Fritjof Helmchen[1] & Winfried Denk[2]

With few exceptions biological tissues strongly scatter light, making high-resolution deep imaging impossible for traditional—including confocal—fluorescence microscopy. Nonlinear optical microscopy, in particular two photon–excited fluorescence microscopy, has overcome this limitation, providing large depth penetration mainly because even multiply scattered signal photons can be assigned to their origin as the result of localized nonlinear signal generation. Two-photon microscopy thus allows cellular imaging several hundred microns deep in various organs of living animals. Here we review fundamental concepts of nonlinear microscopy and discuss conditions relevant for achieving large imaging depths in intact tissue.

Microscopists have always desired to look inside various organ tissues to study structure, function and dysfunction of their cellular constituents. In the past, this has frequently required tissue extraction and histological preparation to gain access. Traditional optical microscopy techniques, which use linear (one-photon) absorption processes for contrast generation, are limited to use near the tissue surface (less than 100 μm) for high-resolution imaging because at greater depths strong and multiple light scattering blurs the images. Scattering particularly strongly affects signal strength in confocal microscopy, which achieves three-dimensional resolution and optical sectioning with a detection pinhole that rejects all light that appears not to originate from the focus.

During the past two decades new optical microscopy techniques have been developed that use nonlinear light-matter interactions to generate signal contrast (reviewed in[1–7]). Nonlinear optical microscopy techniques have special features that make them less sensitive to scattering and thus are well suited for high-resolution imaging in tissues. In particular, two photon–excited fluorescence laser-scanning microscopy (2PLSM)[8], combined with *in vivo* fluorescence labeling techniques, has opened a rapidly expanding field of imaging studies in intact tissues and living animals. Specimens as diverse as lymphatic organs[9,10], kidney[11], heart[12], skin[13] and brain[2,4] can now be examined in detail at depths of up to one millimeter[14], while leaving the tissue intact. Moreover, 2PLSM is used as a tool to study the development, progression and potential treatment of pathological conditions such as tumors[15] and Alzheimer disease[16].

Although 2PLSM by now is a well-established technique, using turn-key laser sources and commercial microscope systems, it remains important to understand the underlying principles and key technical aspects, especially when optimizing a microscope system to achieve large imaging depths. In this review, we discuss physical principles, with special emphasis on imaging-system parameters important for deep imaging, and summarize technical issues regarding the application of 2PLSM for high-resolution imaging in living animals.

NONLINEAR OPTICAL MICROSCOPY

In optical microscopy one can distinguish between linear and nonlinear excitation. Traditional techniques, including confocal microscopy, generate contrast from light-matter interactions, in which the elementary process involves a single photon and which therefore depend linearly on the incident light intensity. Nonlinear techniques are fundamentally different in that they use 'higher-order' light-matter interactions involving multiple photons for contrast generation. The nonlinear nature of these interactions leads to qualitatively new imaging properties.

[1]Department of Neurophysiology, Brain Research Institute, University of Zurich, CH-8057 Zurich, Switzerland. [2]Department of Biomedical Optics, Max Planck Institute for Medical Research, D-69120 Heidelberg, Germany. Correspondence should be addressed to F.H. (helmchen@hifo.unizh.ch) or W.D. (winfried.denk@mpimf-heidelberg.mpg.de).

PUBLISHED ONLINE 18 NOVEMBER 2005; DOI:10.1038/NMETH818

Multiphoton absorption

Several different nonlinear processes can occur when light interacts with matter (Fig. 1). Most widely used in biological imaging is fluorescence excitation by two-photon absorption[17]. Two photons that arrive 'simultaneously' (within ~0.5 fs) at a molecule combine their energies to promote the molecule to an excited state, which then proceeds along the normal fluorescence-emission (or photochemical-reaction) pathway[1,17]. Similarly, three or more photons can combine to cause excitation.

The efficiency of multiphoton absorption depends on physical properties of the molecule (the 'multiphoton absorption cross-section')[5,18], and on the spatial and temporal distribution of the excitation light. Most nonlinear processes have in common that the transition probabilities are extremely low at 'normal' light intensities. To generate sufficient signal, excitation light has to be concentrated in space and time. High spatial densities are (cheaply) generated by focusing a laser beam through a high numerical aperture (NA) objective. Concentration in the time domain requires the use of (expensive) lasers that emit 'ultrashort' pulses (less than a picosecond long) with correspondingly high peak intensities. For laser pulses of width τ occurring at a rate f_R, the signal is enhanced by a factor of $1 / (\tau f_R)^{n-1}$ compared to continuous-wave illumination, where n is the number of photons involved in the elementary process. Lasers typically used in 2PLSM provide 100-fs pulses at about 100 MHz, with a 'two-photon advantage'[1] of about 10^5.

Other nonlinear effects

Multiphoton absorption is but one of several possible nonlinear interactions[7]. Another is optical-harmonic generation, in which two or more photons are 'simultaneously' scattered, generating a single photon of exactly twice (thrice, and so on) the incoming quantum energy (Fig. 1a). Harmonic generation requires no actual absorption but is enhanced near a resonance, albeit at the expense of parasitic absorption[6]. It also differs from multiphoton absorption in that it is a coherent, that is, phase-preserving process, which causes speckles, possible cancellation, predominantly forward-directed emission and supralinear dependence on the chromophore density. In practice, only second-harmonic[6] and third-harmonic generation[19,20] have been used. Second-harmonic (but not third-harmonic) generation depends on the absence of inversion symmetry, which not only requires that individual molecules are inversion-asymmetric (as most biological molecules are) but also that they are spatially ordered. Second-harmonic generation has, therefore, been useful for investigating ordered structural protein assemblies such as collagen fibers[21] or microtubuli[22]. Similarly, dyes that are incorporated preferentially in one leaflet of the plasma membrane can be used to detect membrane voltage[23,24]. A further process used for microscopy is 'coherent anti-Stokes Raman scattering' (Fig. 1a), which is sensitive to molecular vibration states and can be used to detect the presence of specific chemical bond types[25,26].

Why nonlinear is more than linear

All nonlinear microscopy techniques require expensive pulsed laser systems to achieve sufficient excitation rates. Two major advantages make the investment worthwhile. First, because multiple excitation photons combine their quantum energies in nonlinear microscopy, the photons generated (or the transitions excited) have higher energies than the excitation light making emission 'bluer' than the excitation, which is different from traditional fluorescence. For commonly used fluorescent markers, multiphoton absorption occurs in the near-infrared wavelength range (700–1,000 nm), whereas emission occurs in the visible spectral range. Near-infrared light not only penetrates deeper into scattering tissue (Box 1) but is also generally less phototoxic owing to the lack of significant endogenous (one-photon) absorbers in most tissues[27].

The second major advantage of two-photon absorption and, in fact, of all nonlinear contrast mechanisms, is that the signal (S) depends supralinearly ($S \propto I^n$) on the density of photons, that is, the light intensity (I). As a consequence, when focusing the laser beam through a microscope objective, multiphoton absorption is spatially

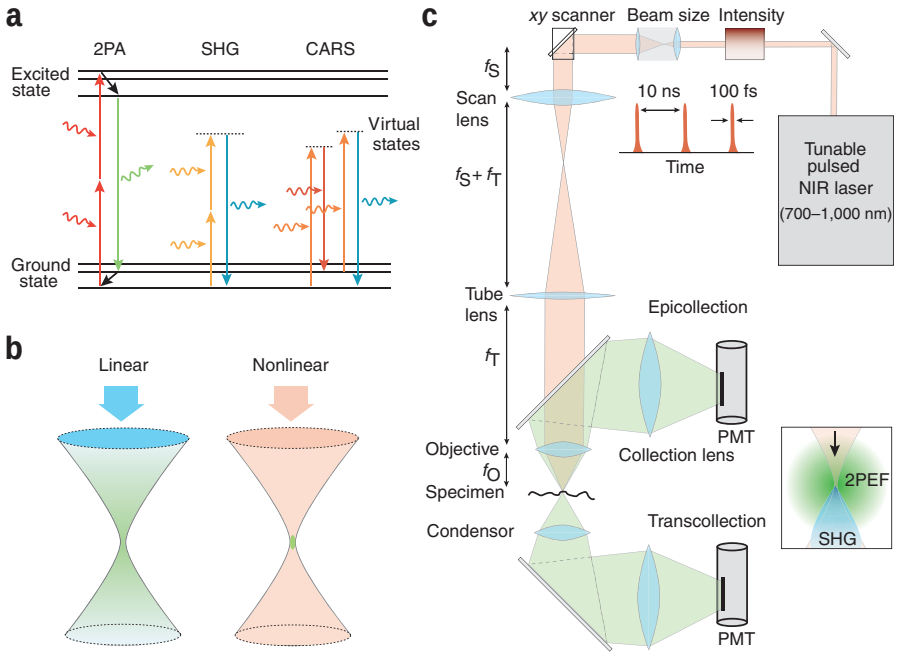

Figure 1 | Nonlinear optical microscopy. (**a**) Jablonski diagram, illustrating two-photon absorption (2PA), second-harmonic generation (SHG) and coherent anti-Stokes Raman scattering (CARS). Note that in second-harmonic generation and Raman scattering no actual electronic excitation takes place. (**b**) Spatial confinement of signal generation with nonlinear excitation. Visible ('blue-ish') light is used for excitation in single-photon microscopy, whereas near-infrared ('red-ish') light is used in 2PLSM. In single-photon microscopy an entire cone of fluorescence light (green) is generated, whereas nonlinear signal production is localized to the vicinity of the focal spot. (**c**) Generic nonlinear laser-scanning microscope. A laser source provides near-infrared ultrashort pulses; intensity and beam size are adjusted before coupling the laser beam to the microscope. The focal lengths of the scan lens (f_S), the tube lens (f_T) and the objective (f_O) are indicated. Two-photon excited fluorescence (2PEF), which is isotropically emitted (inset), can be collected in epi- and/or trans-collection mode, using whole-area detection by photomultiplier tubes (PMTs). Forward-directed optical-harmonic and Raman signals are detected in transcollection mode in transparent samples. For *in vivo* experiments epicollection is used exclusively.

confined to the perifocal region (Fig. 1b). The absence of multiphoton absorption in out-of-focus planes contrasts with confocal microscopy, where (single-photon) absorption occurs within the entire excitation light cone. The lack of out-of-focus excitation in nonlinear microscopy further reduces photodamage and thus increases tissue viability, which is crucial for long-term imaging[28]. Localization of excitation also provides excitation-based three-dimensional resolution with no need for spatially resolved detection through a confocal pinhole. By the same token, multiphoton absorption allows highly localized photomanipulations, such as photobleaching and photolytic release of caged compounds, within femtoliter volumes[29–31], which, however, is beyond the scope of this review.

Localization of excitation is maintained even in strongly scattering tissue because the density of scattered excitation photons generally is too low to generate significant signal, making nonlinear microscopy far less sensitive to light scattering than traditional microscopy (Fig. 2). This is of paramount importance for deep imaging, because it means that all fluorescence photons are known to originate from near the focus and thus can provide useful signal. The best detection strategy therefore becomes: collect as many photons as possible, wherever they seem to come from, but look at their color. Scattering does, however, increase the spatioangular range (the phase space) within which fluorescence light emerges from the tissue so that special detection optics is needed to optimize fluorescence collection from deep foci.

BOX 1 LIGHT SCATTERING IN BIOLOGICAL TISSUE

In most biological tissues absorption of light is negligible compared to scattering, particularly in the near-infrared wavelength range. Scattering is the deflection of a light 'ray' from its original direction; if the photon energy stays unchanged, it is termed 'elastic'. Elastic scattering depends on refractive index inhomogeneities, which are present even in glass but are much stronger in tissue because cells are a heterogeneous mixture of molecules and supramolecular structures with varying molecular polarizabilities. The strength of scattering is described by the 'mean free path' (l_s), the average distance between scattering events. The likelihood and angular distribution of scattering depend on refractive index variation, object size and wavelength λ. For very small objects (such as isolated atoms or molecules in a gas) scattering is nearly isotropic and strongly wavelength-dependent ($\propto \lambda^{-4}$; 'Rayleigh scattering'). For objects comparable in size to the wavelength (as in cells) scattering is directed mostly in the forward direction. This can be quantified by the anisotropy parameter (g) or by the 'transport mean free path', $l_t = l_s / (1 - g)$, which is the distance after which 'direction memory' is lost. Measurements in brain gray matter yielded values for l_s of 50–100 μm at 630 nm in extracted tissue[50,51] and of about 200 μm at 800 nm *in vivo*[43,53]. Scattering decreases with wavelength albeit less than expected for Rayleigh scattering[43]. The anisotropy parameter generally is high (≈0.9) in brain tissue[51].

In nonlinear optical microscopy only ballistic (non-scattered) photons contribute to signal generation in the focal volume. The ballistic power follows a Lambert-Beer–like exponential decline with imaging depth z

$$P_{ball} = P_0 \, e^{-z/l_s} \quad (1)$$

with length constant l_s and surface power P_0. Because of the quadratic intensity-dependence in 2PLSM, the fluorescence signal declines as

$$F_{2PE} \propto (e^{-z/l_s})^2 = e^{-2z/l_s} \quad (2)$$

Conversely, we need an exponentially increasing laser power entering the surface ($P_0 \propto e^{z/l}$) to maintain the same ballistic intensity at the focus. The reduction in focal intensity depends on l_s and not l_t, because even a small deflection from the original path causes a ray to miss the focus (**Fig. 2**). In contrast, the forward-directed angular distribution of scattering is important for the calculation of the near-surface background[103] (P. Theer and W.D., unpublished data). Both l_s and g depend not only on tissue type but can change substantially with age and upon removal of the tissue from the animal[43]. Surface scattering can become important if the beam crosses between media with substantially different refractive indices, for example when imaging through the skull.

Scattering of fluorescence photons is important for the detection process. Because of the short mean free path of visible light, the ballistic fraction becomes quickly irrelevant with increasing focal depth. For sufficient depth, multiply scattered fluorescence light leaves the sample from a diffusely radiating region on the surface, which has a full-width-at-half-maximum intensity (FWHM) of about 1.5× the focal depth, independent of the scattering length[44].

A TWO-PHOTON MICROSCOPE SETUP

In many respects, a 2PLSM is similar to a confocal microscope. The main differences are the excitation laser and the detection pathway. Commercial confocal microscopes can be converted into multiphoton microscopes[8], but major modifications and partial rebuilding may be required to achieve optimal performance, especially for deep imaging. Alternatively, the microscope can be custom built, which is cheaper but requires technical expertise or help from specialized companies. Custom-built microscopes typically lack a microscope corpus, a design that is advantageous for *in vivo* imaging because it provides space for placing the animal, and imposes fewer constraints on the size and position of the detectors. The availability of laser-scanning software[32,33] facilitates such custom designs. Here we only describe the basic microscope design; detailed instructions are available elsewhere[5,33–35].

A multiphoton microscope requires a pulsed laser source (Fig. 1c). Historically, the use of nonlinear light-matter interactions in a microscope only became possible after the development of ultrafast pulsed lasers (for a collection of reprints see 36). Whereas the first two-photon images[8] were taken using a lab-built laser system, suitable near-infrared femtosecond laser systems have now been commercially available for more than a decade. Most widely-used is the Titanium-sapphire (Ti:sapphire) oscillator, with a repetition rate (~100 MHz) that matches typical fluorescence lifetimes, thus balancing excitation efficiency and onset of saturation. The wavelength can

be tuned over a large range (670–1,070 nm), allowing the excitation of many fluorophores used in biology[18]. Key parameters that have to be considered when choosing a laser system are available power at the desired wavelength and pulse length. An optimal pulse length, however, cannot be strictly defined. Depending on the microscope design, relatively short pulses (<100 fs) at the laser output may end up as longer pulses at the sample than initially longer pulses will end up because they are broadened by dispersive optical glass components in the excitation path to a larger extent. Dispersive broadening can be precompensated by a prism or grating arrangement[37,38], thus restoring the initial pulse width at the sample and maximizing two-photon absorption. Another complicating factor is that, at least at high power, photobleaching and photodamage depend more-than-quadratically on excitation intensity[39–41]. Hence, for a given microscope setup and specimen, an optimal pulse length (or even pulse shape[42]) may have to be empirically determined, requiring a compromise between fluorescence yield and photodamage.

Compact Ti:sapphire laser systems are now available, no longer requiring user adjustments and providing computer-controlled wavelength tuning over a broad range. Although these laser systems are more user-friendly than a mercury arc lamp, it is still helpful to understand the characteristics of the laser beam, in particular if one aims to optimize the system for deep imaging. The available output power is one of the limiting factors for the maximum imaging depth but the average power (~1W) provided by these commercial systems over the central portion of the tuning range is sufficient for most applications, even with losses in the optical pathway.

The excitation pathway of a typical multiphoton microscope is as follows (all optics should be optimized for near-infrared light). Starting from the laser, the beam is expanded using a telescope (using either curved mirrors or lenses) followed or preceded by a laser intensity modulator (Fig. 1c). Because the laser beam is linearly polarized, the intensity can be adjusted easily, albeit slowly, by using a $\lambda/2$ waveplate and a polarizer. Alternatively, acousto- or electro-optical devices can be used, providing high extinction ratios and permitting rapid intensity changes. Such devices can also be used to automatically compensate for power loss with depth if the scattering length in the tissue is known (Box 1). The beam is then scanned by a *xy*-deflection module (usually a pair of galvanometric scanners) and further expanded by the combination of scan and tube lens in order to 'fill' the back aperture of the microscope objective, which focuses the light into the sample.

Although the descanned confocal detector pathway (not shown in Fig. 1c) can be used to obtain two photon–excited fluorescence images in clear specimens, clipping at the pinhole will decrease the available signal by several orders of magnitude deep in scattering specimens. Hence a simpler but better detector arrangement is used in nonlinear microscopy to capture as many of the potentially highly scattered signal photons as possible. In most systems a 'whole-area' epi-detection scheme is used, with all light that is collected by the objective also guided onto the detector[1,33,34,43,44]. For small or transparent specimens *trans*-collection through a high-NA condensor can be used instead or, better, in addition, capturing even more light (Fig. 1c). Because of the preferentially forward-directed signal, trans-collection is the principal detection mode in optical-harmonic generation and Raman scattering. In deep, scattering specimens, however, no light will penetrate, and epicollection is the only mode that can be used. Epicollection results in surprisingly little signal loss provided the detector's field of view is large enough because most signal photons eventually leave the tissue surface after multiple scattering events. For optical-harmonic generation and Raman scattering, the detection field of view needs to be especially large because the initially forward-propagating light has to 'turn around' first (Fig. 2).

OPTIMIZATION FOR DEEP IMAGING

We now consider how fluorescence generation and detection can be optimized for deep imaging and what fundamentally limits the imaging depth.

Excitation wavelength

To look deep inside tissue sufficient signal needs to be generated, which means that sufficient light needs to reach the focus without being scattered (the 'ballistic' fraction). Less-scattering long-wavelength light thus should allow deeper penetration (Box 1). The optimal wavelength for deep tissue imaging is, however, also affected by the two-photon absorption spectrum of the fluorophores used and by the fact that less power is available at the extremes of the laser tuning range.

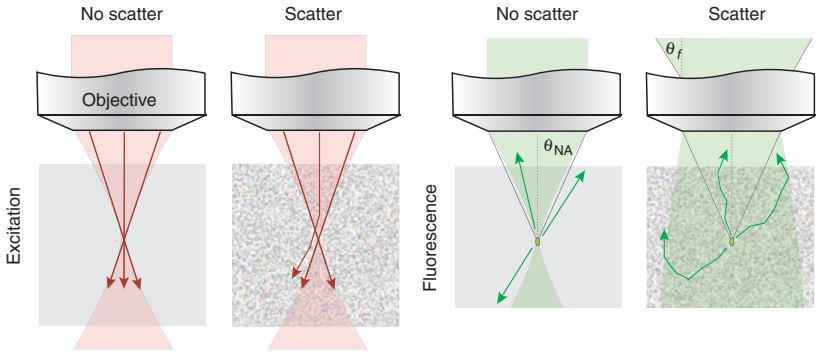

Figure 2 | Signal generation and fluorescence collection in clear tissue (no scatter) and in scattering tissue (scatter). In clear tissue all excitation light reaches the focus, but in scattering tissue, scattering (even by a small angle) causes light rays to miss the focus and be lost to signal generation. This leads to a roughly exponential decrease in excitation with depth. In clear tissue only fluorescence light rays initially emitted into the collection cone, determined by the objective's NA, can be detected, but in scattering tissue fluorescence light is (multiply) scattered and may even 'turn around'. Fluorescence light apparently originates from a large field of view but a larger fraction than in the nonscattering case is actually within the angular acceptance range θ_f of the objective.

Beam size

Loss of excitation power, for example, by clipping at apertures in the light path, lowers the achievable maximum depth. Although many of the lenses in the beam path will allow the passage of larger beams than specified, this is not true for the back aperture of the objective lens, which defines the NA and thus determines the achievable spatial resolution (Box 2). Because the radial intensity profile of a laser beam is Gaussian-shaped, an exact match to an aperture is impossible, and a compromise between resolution and transmitted power has to be found[33]. The width of a Gaussian beam is often defined

BOX 2 IMAGE FORMATION AND SPATIAL RESOLUTION

Image formation in a microscope is described using the image of a point (for example, of a fluorophore), the so-called point-spread function (PSF). The image of any object is obtained convolving the object intensity distribution with the PSF. The three-dimensional PSF depends on the wavelength and the NA and, for an aberration-free lens of circular aperture, is given by[104]

$$\mathrm{PSF}(v,u) = \left| 2\int_0^1 P(\rho)\, J_0(v\rho)\exp(iu\rho^2/2)\rho\, d\rho \right|^2 \qquad (3)$$

J_0 denotes the zero-order Bessel function and $v = k(\mathrm{NA})r$ and $u = k(\mathrm{NA})^2 z$ are radial and axial normalized optical coordinates with the wave number $k = 2\pi / \lambda$. For a confocal microscope the detection pinhole adds a second PSF for the detection side. Assuming an ideal pinhole and similar wavelengths for illumination and fluorescence the effective PSF is

$$\mathrm{PSF}_{\mathrm{confocal}} = \mathrm{PSF}_{\mathrm{illumination}} \times \mathrm{PSF}_{\mathrm{detection}} \approx \mathrm{PSF}^2(v,u) \qquad (4)$$

For 2PLSM with whole-area detection the effective PSF is the square of the illumination PSF

$$\mathrm{PSF}_{\mathrm{two\text{-}photon}} = (\mathrm{PSF}_{\mathrm{illumination}})^2 \approx \mathrm{PSF}^2(v/2, u/2) \qquad (5)$$

with $v/2$ and $u/2$ indicating an about doubled illumination wavelength compared to confocal. Spatial resolution can be quantified using the width of the effective PSF (approximate expressions for PSF widths in 2PLSM are available[5]). Because of the longer excitation wavelength used in 2PLSM, the theoretical PSF width is larger in 2PLSM than in confocal microscopy. In practice, however, the achievable spatial resolutions are similar because finite-sized pinholes have to be used in confocal microscopy, broadening the effective PSF[105].

The resolution also depends on the intensity distribution in the back aperture of the objective and a pupil function $P(\rho)$, which needs to be included (**Fig. 3**). $P(\rho) = 1$ for uniform illumination and is $\exp(-\rho^2 / T^2)$ for a Gaussian beam (T is the fill factor $D_{\mathrm{Beam}} / D_{\mathrm{BA}}$ with D_{Beam} the $1/e^2$-intensity width and D_{BA} the back-aperture diameter).

by where intensity drops to $1/e^2$ (13.7%). With a fill factor of one, defined here as the $1/e^2$-intensity width being equal to the back-aperture diameter, power transmission is 86% (Fig. 3). The lateral and axial resolution (defined, for example, by the 1/e-width of the radial and axial profile of the focal spot[5]) are nearly unchanged in this case compared to uniform illumination (8% and 4% increases, respectively). A further reduction of beam size improves power transmission but broadens the focal volume as the 'effective' NA is reduced (Fig. 3). The resolution loss is, however, smaller than it would be for a 'top-hat' beam because for a Gaussian profile large-angle rays are still present up to the nominal NA of the objective. Note that large-angle rays are more likely to be scattered than central rays simply because they travel a longer distance to the focus, which leads to a reduction of the effective NA with increasing depth in scattering tissue.

For objects that are large compared to the focal volume, a reduction of the effective NA does not lead to a reduction in the total two-photon excited fluorescence[45]; smaller structures will, however, become dimmer. Underfilling the back aperture also lowers the peak intensity, potentially reducing photobleaching and photodamage, which have been found to have a more-than-quadratic intensity dependence in some cases[39–41]. Finally, the narrower light cone of a lower effective NA is less likely to run into obstacles (for example, blood vessels) as it penetrates the tissue.

Pulse width

A complicating factor is that ultrashort pulses are broadened ('dispersed') while propagating in material, reducing the two-photon absorption efficiency. The underlying physical principle is that longer-wavelength ('red') components of the pulse spectrum travel faster in optical materials than short-wavelength ('blue') components, so that the pulse is lengthened and 'chirped' (frequency-modulated). It is possible to compensate for the group-delay dispersion of the

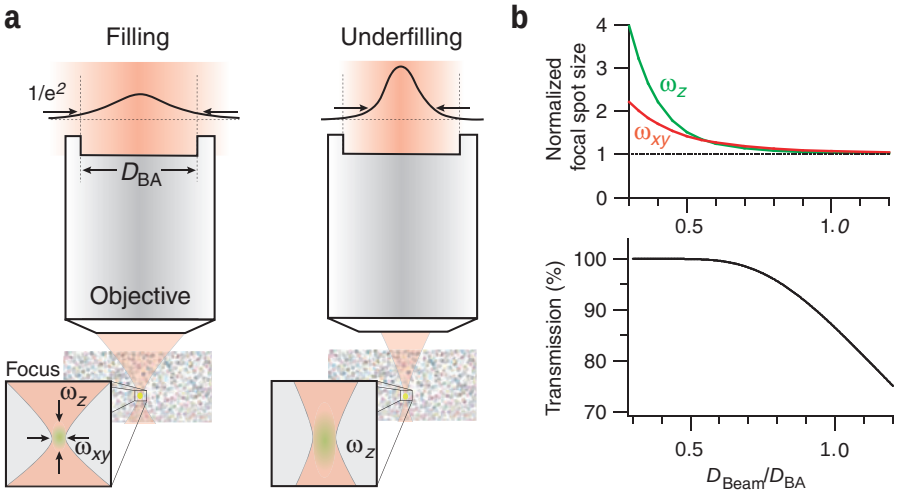

Figure 3 | Beam size adjustment relative to the objective's back aperture. (**a**) 'Matched' filling of the back aperture with an expanded beam (fill factor of one; power transmission 86%; left). In this case most of the NA is used and almost diffraction-limited resolution is reached. Underfilling of the back aperture (right). The beam is expanded less to optimize power transmission. Because a lower effective NA is used, spatial resolution is reduced. (**b**) Focal spot size and power transmission as a function of the fill factor, the ratio between D_{Beam} ($1/e^2$-width) and D_{BA}. Radial width (ω_{xy}) and axial width (ω_z) of the focal volume are normalized to the values for a uniformly filled back aperture. For fill factors around 0.7, nearly all power is transmitted with only minor losses in lateral and axial resolution.

microscope by giving the short-wavelength components a sufficient head start (negative 'prechirp') so that blue and red components arrive at the sample at the same time, restoring as-short-as-possible ('band-limited') pulses at the focus. Such compensation is useful if average power is limiting, for example, because of availability or single photon–induced damage. Prechirping can be achieved by using grating or prism arrangements, which first spatially separate the different-wavelength components, then impose different path lengths, and finally recombine the spectral components. Most commonly the laser beam double-passes a pair of prisms or gratings, the spacing of which determines the amount of negative prechirp[37,38]. A disadvantage of prechirp units is that their optical surfaces can lead to power losses.

Pulse repetition rate

The 'two-photon advantage' can also be increased by lowering f_R while maintaining average power levels. Because in mode-locked lasers f_R is determined by the optical resonator geometry (in most commercial systems around 100 MHz), it cannot easily be changed by a substantial factor. Much reduced repetition rates are provided by regenerative amplifiers, which amplify a submultiple of pulses from an oscillator. As a consequence the peak power is increased by as much as 10^8 in extreme cases at the expense of lowering the repetition rate to around 1 Hz[46]. For imaging applications at least one pulse per pixel is needed, however, limiting the reduction in f_R to about a factor of 1,000 (assuming 10-µs pixel dwell time). This approach can be used to enhance depth penetration[47] and has been demonstrated for *in vivo* imaging[14].

Correcting for tissue inhomogeneities

Signal generation is strongly affected if the focus quality is degraded by distortion of the incoming wave front. Such distortions are due to inhomogeneity of the refractive indices within the tissue, as caused for example by blood vessels or clusters of cell bodies acting as microlenses. Wavefront distortions can—if they can be measured[48]—be corrected[49] by using wave-shaping elements such as deformable mirrors.

Fluorescence collection

As important, or perhaps even more important, as the maximization of signal generation is the optimization of collection and detection efficiencies. Because scattering is more severe for shorter wavelengths, the contribution of ballistic fluorescence photons is minor beyond about one scattering mean-free-path (50–90 µm at 600 nm in brain gray matter[50,51]), and is negligible several hundred microns deep into brain tissue. Hence the confocal detection pathway becomes useless and attention has to be paid to the detection of scattered light, which emerges from the tissue surface spanning an area that is wider than the focus is deep (Fig. 2). Therefore, even with a small imaged field of view, efficient fluorescence detection requires a large detected field of view[43,44]. Because a large field of view corresponds to low magnification, special objectives that combine high NA with low magnification have particularly high collection efficiencies[43]. For a large field of view, the post-objective detection pathway has to be carefully designed to guide all light onto the detector (Fig. 1c). A large spatio-angular spread also rules out the use of certain types of detectors—such as photon-counting avalanche photodiodes, which have some of the highest detection quantum efficiency for fluorescence but a small area—and of spectrometer detectors. *In vivo* two-photon microscopes thus use photomultiplier tubes, available with large sensitive areas and reasonable quantum efficiencies.

The depth limit

The maximum achievable imaging depth is proportional to the scattering mean-free-path and depends logarithmically on available laser power, two-photon advantage and collection efficiency[43]. With a laser oscillator providing ~100-fs pulses, the maximum depth usually is limited by the available average power (1 W average power allows imaging depths of about 600–800 µm in the neocortex)[52–56]. When a regenerative amplifier is used, it is possible to image deeper (up to 1 mm in the neocortex)[14]. Eventually, however, fluorescence generated near the sample surface becomes a limiting factor[14]. The resulting contrast reduction might be impossible to overcome in samples with a wide fluorophore distribution as, for example, in transgenic mice with extensive GFP expression. The achievable imaging depth also strongly depends on other tissue properties such as microvasculature organization, cell body arrangement, collagen or myelin content, which will more-or-less degrade the laser focus and limit signal generation deep inside the tissue. If deeper structures need to be reached and if less-scattered longer wavelengths cannot be used, mechanical penetration or removal[57] of overlying tissue may be necessary. Efforts in this direction have been made using very narrow objective lenses made from gradient-index (GRIN) material[58–61].

LOOKING INSIDE LIVING TISSUE

The special advantages of 2PLSM for imaging deep within intact tissue have led to a rapid expansion of its use in various fields of biological research. 2PLSM is now used for high-resolution imaging in various organs of living animals. Here we summarize additional aspects important for *in vivo* imaging using mainly examples of cellular and subcellular imaging in the intact brain.

In vivo labeling techniques

For fluorescence imaging, structures of interest need to be labeled unless they are autofluorescent[13,62]. *In vivo* labeling techniques for staining cells in living tissues have greatly advanced. 'Traditional' synthetic dyes still are indispensable and can be introduced by a variety of methods: injection into the blood stream to label vasculature, for example, to measure blood flow in the brain[53] or the kidney[11]; filling of individual cells via recording electrodes[52,63] (Fig. 4a); uptake and anterograde transport of dextran-conjugated dyes in axons[64,65]; high-affinity binding of certain dyes to protein aggregates[66]; cell-specific spontaneous uptake of water-soluble dyes[56]; and bulk-loading of membrane-permeable calcium indicators[67]. Cells can also be labeled *ex vivo* and introduced back into mice[10].

Fluorescent proteins can be introduced using molecular genetics (for reviews see[68,69]). Widespread but cell-specific labeling can be achieved in transgenic animals expressing anatomical markers[70] or functional indicators[71,72]. Viral systems allow local expression, either short-term but less cell-specific[73,74], or long-term under control of specific promoters[75]. Different approaches can be combined to achieve multicolor labeling of various tissue elements.

Monitoring cell structure and function

Once cells of interest are labeled, various preparations and procedures can be used to study structural and functional dynamics. For short-term studies of the brain a cranial window is opened above the area of

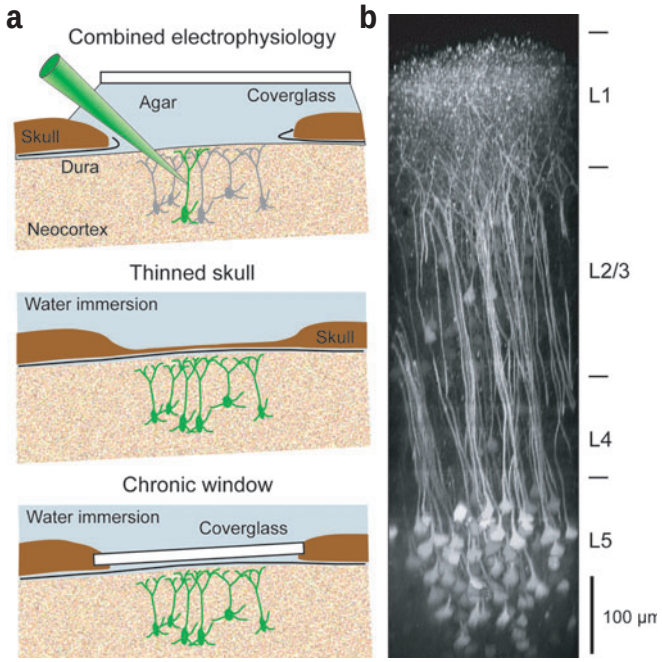

Figure 4 | *In vivo* two-photon imaging in the intact neocortex. (**a**) Different types of brain access. Open cranial window with the *dura mater* removed so that micropipettes for cell labeling and electrophysiological recordings can be inserted (top). Pulsation of the exposed brain is reduced by covering the craniotomy with agar and a coverglass. Thinned-skull (20–40 µm thickness) preparation (middle). Cellular structures are either prelabeled (for example, with fluorescent proteins in transgenic mice) or stained through a tiny hole lateral to the thinned area. Chronically implanted glass window replacing the skull (bottom). Agar is used underneath the window for stabilization. (**b**) Example of deep two-photon imaging in mouse neocortex. Maximum-intensity side projection of a fluorescence image stack, obtained in a transgenic mouse expressing Clomeleon, a genetically-encoded chloride indicator[101], under the control of the Thy1-promoter[102], preferentially in deep layer 5 (L5) pyramidal cells. Data were taken with a 10 W pumped Ti:sapphire oscillator using a 40×, NA 0.8 water-immersion lens (Zeiss). Note that nearly the entire depth of the neocortex can be imaged.

interest, which also provides access for recording electrodes (Fig. 4a). Other organs are surgically exposed in a similar manner or, as in the case of kidney, are exteriorized[11]. A general problem for *in vivo* imaging is motion induced by heart beat and breathing. Therefore, tissue pulsation should be dampened as much as possible, for example, by covering or embedding the exposed organ with agar. Tight control of the anesthesia or artificial respiration can help to alleviate pulsation. For time-lapse imaging of cell structures, we recommend acquiring small subvolumes (image stacks of 10 to 20 focal planes) in anticipation of lateral or focal drift, which can then be corrected offline using correlation methods. Image acquisition can also be synchronized to the heartbeat by triggering individual frames using a simultaneously recorded electrocardiogram, to ensure that all images have the same phase relationship to the heart beat[76].

For long-term imaging over days to months, animals are multiply reanesthetized and image stacks of the same subvolume are acquired. In the brain, these experiments are performed either through the thinned skull[66,77–79] or through a chronically implanted glass window[80–82] (Fig. 4a). In cancer research, a dorsal skin-fold chamber with a glass window is used for imaging implanted tumors[15]. To repeatedly find the same structure (for example, a cell, a blood vessel, an amyloid plaque or even a synapse), stable anatomical landmarks, such as the surface blood vessel pattern can be used.

Functional imaging from neuronal dendrites in the intact neocortex has, so far, still required the introduction of synthetic calcium indicators via electrodes[52,54,55,63,83,84], which has the advantage of providing additional *in vivo* intracellular electrophysiological data. The combination of two-photon optophysiology with electrophysiology[85] will be crucial for studying synaptic integration and single-cell computation in living animals. Great hope still rests on the *in vivo* application of genetically-encoded functional indicators[69,71,72,86,87].

Imaging cellular network dynamics

The ability to label entire cell populations with calcium indicator in living animals, using a rather generally applicable bulk dye-injection method[67], has allowed two-photon imaging of neural and glial network activity with cellular resolution. Somatic and dendritic calcium transients, for example, have revealed spontaneous and evoked activity patterns in the mammalian neocortex[67,88], now with single-spike resolution[89], as well as in the cerebellar cortex[90] and in zebrafish[91,92]. Calcium signals are also found in the neuropil, providing additional information about the input activity in afferent pathways[89,90]. Because bulk-loading does not discriminate well between cell types, specific counterstaining with synthetic or genetically encoded markers may be necessary to highlight particular cell types[56].

Imaging of population activity in neuronal networks pushes present scanning technology to its limit because fast acquisition rates are required to simultaneously measure activity in many cells. Although resonant galvanometric scanners[93] and acousto-optical deflectors[94] can achieve video-rate full-frame acquisition (30 frames/s) of a single optical plane, a further technological challenge is the equally fast recording of cells distributed in three dimensions.

Visualization of pathological states

In vivo imaging is increasingly applied to study tumorgenesis, immune responses and various brain diseases. For example, the evolution of senile Alzheimer disease plaques[66,95], their effects on neighboring neuronal structures[96] and the effectiveness of potential treatments[97] can be followed over months. The ability to image microglial cells in the neocortex opens new possibilities to study their role in a variety of brain diseases[76,98].

CONCLUSIONS AND OUTLOOK

The main strength of 2PLSM and other nonlinear microscopy techniques is the ability to maintain resolution and contrast within scattering tissue. This has permitted, in many fields for the first time, direct visualization of the normal behavior of cells in their natural environment, as well as their response to systematic manipulations. The use of 2PLSM is particularly powerful in neuroscience, where one ultimately wants to correlate cellular activity patterns with the animal's experience and behavior. Moreover, *in vivo* two-photon imaging allows longitudinal studies of structural and functional changes in the same animal over long periods of time (potentially over years). Cellular behavior thus can be put into the larger context, both spatially and temporally.

What will the near future bring? *In vivo* applications of 2PLSM will expand further into other fields, taking advantage of user-friendly laser systems and of ongoing technological developments such as the use of regenerative amplifiers, extended application of optical harmonic generation and other nonlinear effects, and microscope miniaturization. Miniaturized, fiber-based microscopes will allow imaging in freely moving animals[99]. Moreover, flexible submillimeter-sized microscope probes[58–61] may be used to reach deeper into the tissue, beyond the depth limit set by surface-generated background, albeit using a more invasive endoscopic approach. In neuroscience, the direct optical measurement of electrical potentials using two-photon excitation of voltage-sensing dyes[100] or second-harmonic signals[23,24] could have a large impact.

ACKNOWLEDGMENTS

We thank T. Kuner, G. Augustine and G. Feng for providing the Clomeleon mouse and W. Göbel for help with numerical calculations.

COMPETING INTERESTS STATEMENT

The authors declare competing financial interests (see the *Nature Methods* website for details).

Published online at http://www.nature.com/naturemethods/
Reprints and permissions information is available online at http://npg.nature.com/reprintsandpermissions/

1. Denk, W., Piston, D.W. & Webb, W.W. Two-photon molecular excitation in laser-scanning microscopy. In *Handbook of Biological Confocal Microscopy* 2nd edn. (ed. Pawley, J.B.) 445–458 (Plenum Press, New York, 1995).
2. Denk, W. & Svoboda, K. Photon upmanship: why multiphoton imaging is more than a gimmick. *Neuron* **18**, 351–357 (1997).
3. So, P.T., Dong, C.Y., Masters, B.R. & Berland, K.M. Two-photon excitation fluorescence microscopy. *Annu. Rev. Biomed. Eng.* **2**, 399–429 (2000).
4. Helmchen, F. & Denk, W. New developments in multiphoton microscopy. *Curr. Opin. Neurobiol.* **12**, 593–601 (2002).
5. Zipfel, W.R., Williams, R.M. & Webb, W.W. Nonlinear magic: multiphoton microscopy in the biosciences. *Nat. Biotechnol.* **21**, 1369–1377 (2003).
6. Campagnola, P.J. & Loew, L.M. Second-harmonic imaging microscopy for visualizing biomolecular arrays in cells, tissues and organisms. *Nat. Biotechnol.* **21**, 1356–1360 (2003).
7. Mertz, J. Nonlinear microscopy: new techniques and applications. *Curr. Opin. Neurobiol.* **14**, 610–616 (2004).
8. Denk, W., Strickler, J.H. & Webb, W.W. Two-photon laser scanning fluorescence microscopy. *Science* **248**, 73–76 (1990).
9. Cahalan, M.D., Parker, I., Wei, S.H. & Miller, M.J. Real-time imaging of lymphocytes *in vivo*. *Curr. Opin. Immunol.* **15**, 372–377 (2003).
10. Bousso, P. & Robey, E.A. Dynamic behavior of T cells and thymocytes in lymphoid organs as revealed by two-photon microscopy. *Immunity* **21**, 349–355 (2004).
11. Molitoris, B.A. & Sandoval, R.M. Intravital multiphoton microscopy of dynamic renal processes. *Am. J. Physiol. Renal Physiol.* **288**, F1084–F1089 (2005).
12. Rubart, M. Two-photon microscopy of cells and tissue. *Circ. Res.* **95**, 1154–1166 (2004).
13. Laiho, L.H., Pelet, S., Hancewicz, T.M., Kaplan, P.D. & So, P.T. Two-photon 3-D mapping of *ex vivo* human skin endogenous fluorescence species based on fluorescence emission spectra. *J. Biomed. Opt.* **10**, 024016 (2005).
14. Theer, P., Hasan, M.T. & Denk, W. Two-photon imaging to a depth of 1000 microns in living brains by use of a Ti:Al2O3 regenerative amplifier. *Opt. Lett.* **28**, 1022–1024 (2003).
15. Jain, R.K., Munn, L.L. & Fukumura, D. Dissecting tumour pathophysiology using intravital microscopy. *Nat. Rev. Cancer* **2**, 266–276 (2002).
16. Skoch, J., Hickey, G.A., Kajdasz, S.T., Hyman, B.T. & Bacskai, B.J. *In vivo* imaging of amyloid-beta deposits in mouse brain with multiphoton microscopy. *Methods Mol. Biol.* **299**, 349–363 (2005).
17. Goeppert-Mayer, M. *Über Elementarakte mit zwei Quantensprüngen* (On elementary processes with two quantum steps) *Ann. Phys.* **9**, 273–294 (1931).
18. Xu, C. & Webb, W.W. Measurement of two-photon excitation cross sections of molecular fluorophores with data from 690 to 1,050 nm. *J. Opt. Soc. Am. B* **13**, 481–491 (1996).
19. Squier, J., Muller, M., Brakenhoff, G. & Wilson, K. Third harmonic generation microscopy. *Opt. Express* **3**, 315–324 (1998).
20. Oron, D. *et al.* Depth-resolved structural imaging by third-harmonic generation microscopy. *J. Struct. Biol.* **147**, 3–11 (2004).
21. Mohler, W., Millard, A. & Campagnola, P. Second harmonic generation imaging of endogenous structural proteins. *Methods* **29**, 97–109 (2003).
22. Dombeck, D.A. *et al.* Uniform polarity microtubule assemblies imaged in native brain tissue by second-harmonic generation microscopy. *Proc. Natl. Acad. Sci. USA* **100**, 7081–7086 (2003).
23. Bouevitch, O., Lewis, A., Pinevsky, I., Wuskell, J. & Loew, L. Probing membrane-potential with nonlinear optics. *Biophys. J.* **65**, 672–679 (1993).
24. Moreaux, L., Sandre, O., Blanchard-Desce, M. & Mertz, J. Membrane imaging by simultaneous second-harmonic generation and two-photon microscopy. *Opt. Lett.* **25**, 320–322 (2000).
25. Cheng, J., Volkmer, A. & Xie, X. Theoretical and experimental characterization of coherent anti-Stokes Raman scattering microscopy. *J. Opt. Soc. Am. B* **19**, 1363–1375 (2002).
26. Wang, H., Fu, Y., Zickmund, P., Shi, R. & Cheng, J. Coherent anti-stokes Raman scattering imaging of axonal myelin in live spinal tissues. *Biophys. J.* **89**, 581–591 (2005).
27. Svoboda, K. & Block, S.M. Biological applications of optical forces. *Annu. Rev. Bioph. Biomol. Struct.* **23**, 247–285 (1994).
28. Squirrell, J.M., Wokosin, D.L., White, J.G. & Bavister, B.D. Long-term two-photon fluorescence imaging of mammalian embryos without compromising viability. *Nat. Biotechnol.* **17**, 763–767 (1999).
29. Denk, W. Two-photon scanning photochemical microscopy: mapping ligand-gated ion channel distributions. *Proc. Natl. Acad. Sci. USA* **91**, 6629–6633 (1994).
30. Svoboda, K., Tank, D.W. & Denk, W. Direct measurement of coupling between dendritic spines and shafts. *Science* **272**, 716–719 (1996).
31. Matsuzaki, M. *et al.* Dendritic spine geometry is critical for AMPA receptor expression in hippocampal CA1 pyramidal neurons. *Nat. Neurosci.* **4**, 1086–1092 (2001).
32. Pologruto, T.A., Sabatini, B.L. & Svoboda, K. ScanImage: flexible software for operating laser scanning microscopes. *Biomed. Eng. Online* **2**, 13 (2003).
33. Tsai, P.S. *et al.* Principles, design, and construction of a two-photon laser scanning microscope for *in vitro* and *in vivo* brain imaging. *In Vivo Pptical Imaging of Brain Function*. (Frostig, R.D., ed.) (CRC Press, New York, 2002).
34. Mainen, Z.F. *et al.* Two-photon imaging in living brain slices. *Methods* **18**, 231–239 (1999).
35. Majewska, A., Yiu, G. & Yuste, R. A custom-made two-photon microscope and deconvolution system. *Pflugers Arch.* **441**, 398–408 (2000).
36. Gosnell, T.R. & Taylor, A.J. (eds.) *Selected Papers on Ultrafast Laser Technology.* (SPIE Optical Engineering Press, Bellingham, 1991).
37. Treacy, E.B. Optical pulse compression with diffraction gratings. *IEEE J. Quantum Electron.* **5**, 454–458 (1969).
38. Diels, J.-C.M., Fontaine, J.J., McMichael, I.C. & Simoni, F. Control and measurement of ultrashort pulse shapes (in amplitude and phase) with femtosecond accuracy. *App. Opt.* **24**, 1270–1282 (1985).
39. Patterson, G.H. & Piston, D.W. Photobleaching in two-photon excitation microscopy. *Biophys. J.* **78**, 2159–2162 (2000).
40. Hopt, A. & Neher, E. Highly nonlinear photodamage in two-photon fluorescence microscopy. *Biophys. J.* **80**, 2029–2036 (2001).
41. Koester, H.J., Baur, D., Uhl, R. & Hell, S.W. Ca^{2+} fluorescence imaging with pico- and femtosecond two-photon excitation: signal and photodamage. *Biophys. J.* **77**, 2226–2236 (1999).
42. Kawano, H. *et al.* Attenuation of photobleaching in two-photon excitation fluorescence from green fluorescent protein with shaped excitation pulses. *Biochem. Biophys. Res. Commun.* **311**, 592–596 (2003).
43. Oheim, M., Beaurepaire, E., Chaigneau, E., Mertz, J. & Charpak, S. Two-photon microscopy in brain tissue: parameters influencing the imaging depth. *J. Neurosci. Methods* **111**, 29–37 (2001).
44. Beaurepaire, E. & Mertz, J. Epifluorescence collection in two-photon microscopy. *Appl. Opt.* **41**, 5376–5382 (2002).
45. Birge, R.R. 2-photon spectroscopy of protein-bound chromophors. *Acc. Chem. Res.* **19**, 138–146 (1986).
46. Wang, H. *et al.* Generation of 10-W average-power, 40-TW peak-power, 24-fs pulses from a Ti:sapphire amplifier system. *J. Opt. Soc. Am. B* **16**, 1790–1794 (1999).
47. Beaurepaire, E., Oheim, M. & Mertz, J. Ultra-deep two-photon fluorescence excitation in turbid media. *Opt. Comm.* **188**, 25–29 (2001).
48. Feierabend, M., Ruckel, M. & Denk, W. Coherence-gated wave-front sensing in strongly scattering samples. *Opt. Lett.* **29**, 2255–2257 (2004).
49. Booth, M., Neil, M., Juskaitis, R. & Wilson, T. Adaptive aberration correction in a confocal microscope. *Proc. Natl. Acad. Sci. USA* **99**, 5788–5792 (2002).
50. Taddeucci, A., Martelli, F., Barilli, M., Ferrari, M. & Zaccanti, G. Optical properties of brain tissue. *J. Biomed. Opt.* **1**, 117–123 (1996).

51. Yaroslavsky, A. *et al.* Optical properties of selected native and coagulated human brain tissues *in vitro* in the visible and near infrared spectral range. *Phys. Med. Biol.* **47**, 2059–2073 (2002).
52. Svoboda, K., Denk, W., Kleinfeld, D. & Tank, D.W. *In vivo* dendritic calcium dynamics in neocortical pyramidal neurons. *Nature* **385**, 161–165 (1997).
53. Kleinfeld, D., Mitra, P.P., Helmchen, F. & Denk, W. Fluctuations and stimulus-induced changes in blood flow observed in individual capillaries in layers 2 through 4 of rat neocortex. *Proc. Natl. Acad. Sci. USA* **95**, 15741–15746 (1998).
54. Svoboda, K., Helmchen, F., Denk, W. & Tank, D.W. Spread of dendritic excitation in layer 2/3 pyramidal neurons in rat barrel cortex *in vivo*. *Nat. Neurosci.* **2**, 65–73 (1999).
55. Helmchen, F., Svoboda, K., Denk, W. & Tank, D.W. *In vivo* dendritic calcium dynamics in deep-layer cortical pyramidal neurons. *Nat. Neurosci.* **2**, 989–996 (1999).
56. Nimmerjahn, A., Kirchhoff, F., Kerr, J.N. & Helmchen, F. Sulforhodamine 101 as a specific marker of astroglia in the neocortex *in vivo*. *Nat. Methods* **1**, 31–37 (2004).
57. Mizrahi, A., Crowley, J., Shtoyerman, E. & Katz, L. High-resolution *in vivo* imaging of hippocampal dendrites and spines. *J. Neurosci.* **24**, 3147–3151 (2004).
58. Jung, J. & Schnitzer, M. Multiphoton endoscopy. *Opt. Lett.* **28**, 902–904 (2003).
59. Levene, M., Dombeck, D., Kasischke, K., Molloy, R. & Webb, W. *In vivo* multiphoton microscopy of deep brain tissue. *J. Neurophysiol.* **91**, 1908–1912 (2004).
60. Jung, J., Mehta, A., Aksay, E., Stepnoski, R. & Schnitzer, M. *In vivo* mammalian brain Imaging using one- and two-photon fluorescence microendoscopy. *J. Neurophysiol.* **92**, 3121–3133 (2004).
61. Göbel, W., Kerr, J.N., Nimmerjahn, A. & Helmchen, F. Miniaturized two-photon microscope based on a flexible coherent fiber bundle and a gradient-index lens objective. *Opt. Lett.* **29**, 2521–2523 (2004).
62. Huang, S., Heikal, A.A. & Webb, W.W. Two-photon fluorescence spectroscopy and microscopy of NAD(P)H and flavoprotein. *Biophys. J.* **82**, 2811–2825 (2002).
63. Waters, J., Larkum, M., Sakmann, B. & Helmchen, F. Supralinear Ca^{2+} influx in dendritic tufts of layer 2/3 neocortical pyramidal neurons *in vitro* and *in vivo*. *J. Neurosci.* **23**, 8558–8567 (2003).
64. Wachowiak, M., Denk, W. & Friedrich, R.W. Functional organization of sensory input to the olfactory bulb glomerulus analyzed by two-photon calcium imaging. *Proc. Natl. Acad. Sci. USA* **101**, 9097–9102 (2004).
65. Kreitzer, A., Gee, K., Archer, E. & Regehr, W. Monitoring presynaptic calcium dynamics in projection fibers by *in vivo* loading of a novel calcium indicator. *Neuron* **27**, 25–32 (2000).
66. Christie, R.H. *et al.* Growth arrest of individual senile plaques in a model of Alzheimer's disease observed by *in vivo* multiphoton microscopy. *J. Neurosci.* **21**, 858–864 (2001).
67. Stosiek, C., Garaschuk, O., Holthoff, K. & Konnerth, A. *In vivo* two-photon calcium imaging of neuronal networks. *Proc. Natl. Acad. Sci. USA* **100**, 7319–7324 (2003).
68. Young, P. & Feng, G. Labeling neurons *in vivo* for morphological and functional studies. *Curr. Opin. Neurobiol.* **14**, 642–646 (2004).
69. Miesenbock, G. Genetic methods for illuminating the function of neural circuits. *Curr. Opin. Neurobiol.* **14**, 395–402 (2004).
70. Feng, G. *et al.* Imaging neuronal subsets in transgenic mice expressing multiple spectral variants of GFP. *Neuron* **28**, 41–51 (2000).
71. Hasan, M.T. *et al.* Functional fluorescent Ca^{2+} indicator proteins in transgenic mice under TET control. *PLoS Biol.* **2**, e163 (2004).
72. Wang, J.W., Wong, A.M., Flores, J., Vosshall, L.B. & Axel, R. Two-photon calcium imaging reveals an odor-evoked map of activity in the fly brain. *Cell* **112**, 271–282 (2003).
73. Kim, J. *et al.* Sindbis vector SINrep(nsP2S726): a tool for rapid heterologous expression with attenuated cytotoxicity in neurons. *J. Neurosci. Methods* **133**, 81–90 (2004).
74. Lendvai, B., Stern, E.A., Chen, B. & Svoboda, K. Experience-dependent plasticity of dendritic spines in the developing rat barrel cortex *in vivo*. *Nature* **404**, 876–881 (2000).
75. Dittgen, T. *et al.* Lentivirus-based genetic manipulations of cortical neurons and their optical and electrophysiological monitoring *in vivo*. *Proc. Natl. Acad. Sci. USA* **101**, 18206–18211 (2004).
76. Nimmerjahn, A., Kirchhoff, F. & Helmchen, F. Resting microglial cells are highly dynamic surveillants of brain parenchyma *in vivo*. *Science* **308**, 1314–1318 (2005).
77. Grutzendler, J., Kasthuri, N. & Gan, W.B. Long-term dendritic spine stability in the adult cortex. *Nature* **420**, 812–816 (2002).
78. Yoder, E.J. & Kleinfeld, D. Cortical imaging through the intact mouse skull using two-photon excitation laser scanning microscopy. *Microsc. Res. Tech.* **56**, 304–305 (2002).
79. Zuo, Y., Lin, A., Chang, P. & Gan, W.B. Development of long-term dendritic spine stability in diverse regions of cerebral cortex. *Neuron* **46**, 181–189 (2005).
80. Trachtenberg, J.T. *et al.* Long-term *in vivo* imaging of experience-dependent synaptic plasticity in adult cortex. *Nature* **420**, 788–794 (2002).
81. Majewska, A. & Sur, M. Motility of dendritic spines in visual cortex *in vivo*: changes during the critical period and effects of visual deprivation. *Proc. Natl. Acad. Sci. USA* **100**, 16024–16029 (2003).
82. Holtmaat, A.J. *et al.* Transient and persistent dendritic spines in the neocortex *in vivo*. *Neuron* **45**, 279–291 (2005).
83. Waters, J. & Helmchen, F. Boosting of action potential backpropagation by neocortical network activity *in vivo*. *J. Neurosci.* **24**, 11127–11136 (2004).
84. Charpak, S., Mertz, J., Beaurepaire, E., Moreaux, L. & Delaney, K. Odor-evoked calcium signals in dendrites of rat mitral cells. *Proc. Natl. Acad. Sci. USA* **98**, 1230–1234 (2001).
85. Margrie, T.W. *et al.* Targeted whole-cell recordings in the mammalian brain *in vivo*. *Neuron* **39**, 911–918 (2003).
86. Kerr, R. *et al.* Optical imaging of calcium transients in neurons and pharyngeal muscle of *C. elegans*. *Neuron* **26**, 583–594 (2000).
87. Reiff, D.F. *et al.* *In vivo* performance of genetically encoded indicators of neural activity in flies. *J. Neurosci.* **25**, 4766–4778 (2005).
88. Ohki, K., Chung, S., Ch'ng, Y., Kara, P. & Reid, R. Functional imaging with cellular resolution reveals precise micro-architecture in visual cortex. *Nature* **433**, 597–603 (2005).
89. Kerr, J.N., Greenberg, D. & Helmchen, F. Imaging input and output of neocortical networks *in vivo*. *Proc. Natl. Acad. Sci. USA* **102**, 14063–14068 (2005).
90. Sullivan, M.R., Nimmerjahn, A., Sarkisov, D.V., Helmchen, F. & Wang, S.S.-H. *In vivo* calcium imaging of circuit activity in cerebellar cortex. *J. Neurophysiol.* **94**, 1636–1644 (2005).
91. Brustein, E., Marandi, N., Kovalchuk, Y., Drapeau, P. & Konnerth, A. "*In vivo*" monitoring of neuronal network activity in zebrafish by two-photon Ca^{2+} imaging. *Pflugers Arch.* **446**, 766–773 (2003).
92. Niell, C.M. & Smith, S.J. Functional imaging reveals rapid development of visual response properties in the zebrafish tectum. *Neuron* **45**, 941–951 (2005).
93. Fan, G.Y. *et al.* Video-rate scanning two-photon excitation fluorescence microscopy and ratio imaging with cameleons. *Biophys. J.* **76**, 2412–2420 (1999).
94. Roorda, R.D., Hohl, T.M., Toledo-Crow, R. & Miesenbock, G. Video-rate nonlinear microscopy of neuronal membrane dynamics with genetically encoded probes. *J. Neurophysiol.* **92**, 609–621 (2004).
95. Bacskai, B.J. *et al.* Four-dimensional multiphoton imaging of brain entry, amyloid binding, and clearance of an amyloid-beta ligand in transgenic mice. *Proc. Natl. Acad. Sci. USA* **100**, 12462–12467 (2003).
96. Tsai, J., Grutzendler, J., Duff, K. & Gan, W. Fibrillar amyloid deposition leads to local synaptic abnormalities and breakage of neuronal branches. *Nat. Neurosci.* **7**, 1181–1183 (2004).
97. Lombardo, J.A. *et al.* Amyloid-beta antibody treatment leads to rapid normalization of plaque-induced neuritic alterations. *J. Neurosci.* **23**, 10879–10883 (2003).
98. Davalos, D. *et al.* ATP mediates rapid microglial response to local brain injury *in vivo*. *Nat. Neurosci.* **8**, 752–758 (2005).
99. Helmchen, F., Fee, M.S., Tank, D.W. & Denk, W. A miniature head-mounted two-photon microscope. high-resolution brain imaging in freely moving animals. *Neuron* **31**, 903–912 (2001).
100. Kuhn, B., Fromherz, P. & Denk, W. High sensitivity of Stark-shift voltage-sensing dyes by one- or two-photon excitation near the red spectral edge. *Biophys. J.* **87**, 631–639 (2004).
101. Kuner, T. & Augustine, G.J. A genetically encoded ratiometric indicator for chloride: Capturing chloride transients in cultured hippocampal neurons. *Neuron* **27**, 447–459 (2000).
102. Berglund, K., Dunbar, R.L., Psyche, L., Feng, G. & Augustine, G.J. A practical guide: Imaging synaptic inhibition with Clomeleon, a genetically encoded indicator. in *Imaging in Neuroscience and Development: a Laboratory Manual.* (Yuste, R. & Konnerth, A. eds.) (Cold Spring Harbor Press, Cold Spring Harbor, 2005).
103. Ying, J., Liu, F. & Alfano, R. Effect of scattering on nonlinear optical scanning microscopy imaging of highly scattering media. *App. Opt.* **39**, 509–514 (2000).
104. Sheppard, C.J. & Gu, M. Image formation in two-photon fluorescence microscopy. *Optik* **86**, 104–106 (1990).
105. Cox, G. & Sheppard, C.J. Practical limits of resolution in confocal and non-linear microscopy. *Microsc. Res. Tech.* **63**, 18–22 (2004).